Available online at www.sciencedirect.com
ScienceDirect
Journal of the European Ceramic Society 30 (2010) 3013–3021
www.elsevier.com/locate/jeurceramsoc

Partial wick-debinding of low-pressure powder injection-moulded ceramic parts

Lovro Gorjan [a,b,*], Aleš Dakskobler [a], Tomaž kosmač [a]

[a] *Jožef Stefan Institute, Jamova 39, Ljubljana, Slovenia*
[b] *Hidria AET, Poljubinj 89a, Tolmin, Slovenia*

Received 15 April 2010; received in revised form 9 June 2010; accepted 1 July 2010
Available online 25 July 2010

Abstract

Al_2O_3-based green bodies were shaped using low-pressure injection moulding. The binder content and the binder distribution during the thermal debinding inside a wicking embedment were analyzed. A distinct trailing front, which separates the binder-lean and binder-rich regions, was observed. This kind of binder distribution forms suddenly, after the moulded piece is heated above the melting point of the binder and is then cooled down. Mechanisms that can explain the observations are presented. The non-uniform binder distribution is explained by a capillary extraction of the binder with two different mobilities, which depend on the size of the pores inside the moulded piece. A sudden loss of binder at the beginning of the debinding process is the result of exudation, caused by a large thermal expansion of the binder as it melts. During cooling, the binder solidifies, which significantly affects the binder distribution due to a contraction of the binder.

Keywords: Al_2O_3; Injection moulding; Capillary extraction

1. Introduction

Powder injection moulding (PIM) is a net-shape or near-net-shape forming technique, which is most appropriate for producing complex-shaped, low-cost and high-performance products. Low-pressure injection moulding (LPIM) is a variant of PIM, where lower temperatures (typically <100 °C) and much lower pressures (<0.7 MPa) are used in comparison with a conventional high-pressure injection moulding (HPIM), where temperatures typically in the range of 130–190 °C and pressures from 1.4 to 60 MPa are used.[1] The suspension for LPIM should have a low viscosity to allow easy injection into the mould cavity at low-pressures. This is achieved by using a single-component binder with a low melting point – typically a paraffin-wax. The challenging and time-consuming operation in the PIM process is removing the binder from the moulded pieces prior to sintering, without causing any deformation or cracks. This debinding step is usually achieved by slowly heating the pieces, causing the binder to decompose and vaporize. The difficulties are especially large in the LPIM variant, since the binder does not contain a backbone polymer that would hold the particles firmly in place during the debinding. Also, because the binder is a single-component, it melts over a narrow temperature range, at which point the pieces become soft and deformable. An effective way of avoiding the formation of defects is to introduce an additional debinding step – debinding in a wicking embedment (known as wick-debinding). The wicking embedment is a highly porous powder that serves as a physical support for the pieces and also takes an active role in the debinding by capillary suction of the molten binder. The result is a partially debinded body with a developed open porosity. Complete binder removal can be subsequently achieved during the heating to the sintering temperature, by burning and evaporation of the residual binder.

Theoretical work has been done on the wick-debinding by several authors.[2–7] Some of it was based on experiments using HPIM.[3,4] However, they are quite general and can also be applied for the LPIM system. Theoretical work based on experiments using a single-component binder, which is characteristic for LPIM, has also been conducted.[5–7]

The existing theoretical models predict different behaviors during the debinding and many contradict each other. In 1987,

* Corresponding author at: Jožef Stefan Institute, Engineering Ceramics Department, Jamova 39, 1000 Ljubljana, Slovenia. Tel.: +386 40355801.
E-mail address: lovro.gorjan@gmail.com (L. Gorjan).

0955-2219/$ – see front matter © 2010 Elsevier Ltd. All rights reserved.
doi:10.1016/j.jeurceramsoc.2010.07.011

German[2] proposed a model where he assumed that the binder is extracted from a moulded compact as a continuous body in liquid form, leaving behind a region with an irreducible amount of binder. However, the model does not explicitly incorporate any quantity describing the amount of irreducible binder. A partially debinded compact should, therefore, have a characteristic binder distribution with a binder-saturated region near the contact with the wicking powder and a region with no binder on the other side. A sharp border between these regions should be present – a sign of the trailing front of the molten binder. This model is simple and has frequently been used as a basis for research in wick-debinding. Monte-Carlo simulations of binder removal based on German's assumptions have also been conducted.[8,9] The simulations focused on binder penetration in the wicking embedment and examined the case where pieces are not completely surrounded by the embedment.[8,9] German's model has, however, been criticized, on the basis of experimental data. Contradicting the model, many researchers observed that the binder is uniformly distributed inside the body at all stages of the debinding process.[6,7,11,12] Recently a model of wick-debinding has been presented for LPIM, which agrees well with their experimental data for zirconia-wax green bodies. They observed very uniform distribution of the binder within green bodies at all times of the process. Importantly to note is that they used a very coarse ceramic powders with mean particle size of 47 μm.[7]

There is also the question of how can the air enter behind the trailing front into the binder-free region if the moulded pieces are completely surrounded by the wick.[7] Furthermore, the debinding rate did not correspond well to some experiments.[4] It has also been observed that the permeability in a wick embedment can have important effects and can be a limiting factor, rather than the flow through a sample, as was suggested in German's model.[4,7] With more precise examinations of the binder removal rate it has been confirmed that wick-debinding must take place via more than a single mechanism.[6,10,11] One clearly observable effect is a rapid decrease in the binder content at the beginning of the process. This has been attributed to the pressure arising from the thermal expansion of the binder,[10] although the authors did not explain this effect in detail. The exudation due to thermal expansion was considered in the paper of Somasundram et al.[7]

In this paper we report on the wick-debinding of low-pressure injection-moulded alumina parts. A non-uniform binder distribution with a trailing front of melted binder that separates the binder-rich and binder-lean regions does form in the case of alumina powder and paraffin-wax binder LPIM pieces. This finding supports some features of German's original model, but since the model cannot fully explain our observations we propose some modifications to the model. The object of this paper is to recognize and quantify the mechanisms governing the wick-debinding of the LPIM moulded pieces that could explain all the details of our experimental work. In order to verify the theory, we developed a mathematical model, which can be applied using practical conditions, such as a gradual increase in the temperature during the debinding process. Quantities such as the binder content and the binder distribution can be calculated and then directly compared with the experimental data.

2. Experimental procedure

A feedstock was prepared from a powder containing 96% alumina (d_{10} = 0.7 μm, d_{50} = 1.9 μm, d_{10} = 4.2 μm) and 4% steatite (d_{10} = 0.7 μm, d_{50} = 4.8 μm, d_{90} = 9.5 μm) and a paraffin-wax binder, with a melting point of 60 °C. Stearic acid, in the amount of 0.25%, was added as a surfactant to improve the rheological properties relative to the mass of the powder. Two suspensions with different solids loadings were prepared: suspension A, with 87.8%; and suspension B, with 88.0% of powder content. The difference was unintentional. The second suspension was prepared after the model was formulated and the parameters were set, in order to subsequently test the predictions of the model. The suspensions were homogenized in a ball mill at 80 °C for 4 h. The samples were then low-pressure injection-moulded into a cylindrical-shaped mould die with a length of 60 mm and a diameter of 10 mm. The temperature of the suspension during moulding was 65 °C and the pressure was 0.5 MPa. The temperature of the steel mould was in the range 25–30 °C. The linear shrinkage of the suspension inside the mould during the solidification was 1%.

The thermal wick-debinding was performed in a thin-walled aluminum container, filled with a highly porous alumina embedding powder (d_{50} (granules) ≈80 μm), with a surface area of 25 m^2/g, as measured by the BET method. The samples were buried inside the embedment. Each sample had at least a 1 cm-thick embedment in all directions around it. The debinding was performed inside a ventilated oven in an air atmosphere in a controlled temperature regime. This temperature regime was linear:

$$T = T_0 + \frac{\Delta T}{\Delta t} t; \quad \text{for } T \langle T_{\text{dwell}} \tag{1a}$$

$$T = T_{\text{dwell}}; \text{ untill the end} \tag{1b}$$

where T[°C] is the temperature, t[s] is the time, T_0 = 25 °C is the starting temperature, $\Delta T/\Delta t$ = 0.7 or 0.2 K/min is the ramp (two different ramps were used) and T_{dwell} = 130 or 200 °C is the dwell temperature. Two different dwell temperatures were used, which means that in total, four different combinations of ramp and dwell temperatures were applied.

After the debinding the samples were broken and the fracture surfaces were examined with a stereomicroscope. The amount of binder in the binder-rich and binder-lean regions was determined from the mass loss during a complete binder burnout in air at 650 °C.

The porosity of the samples (E_1) was determined from the mass and the dimensions of completely debinded parts. The porosity of the wicking embedment was determined from the density of the powder embedment, determined from volume measurements using a graduated cylinder. The viscosity of the paraffin-wax was measured with a rheometer in the temperature range 80–180 °C. Newtonian behavior was assumed. The density of the molten paraffin was determined from volume measurements at different temperatures (60–180 °C), using a graduated cylinder. The density of the solid paraffin was deter-

mined using Archimedes' method, using pure ethanol as an immersing medium.

For comparison, some of the samples were heated above the melting point of the binder without wick embedment and then quenched in liquid nitrogen. In this way we could indirectly observe what the binder distribution was like when the binder was in the molten state.

3. Experimental results

The fracture surfaces of samples debinded for different debinding times, photographed with a stereomicroscope, are shown in Fig. 1. From the pictures it is clear how the binder distribution evolved during the debinding. The brighter, inner part of the fracture surface is a binder-depleted core, surrounded by a binder-rich region, which can be identified as being darker-gray in the pictures. The trailing front, which separates the two regions, is moving towards the edge of the sample during the debinding. It is well defined, especially later on in the process.

Degree of saturation, defined as the ratio of the volume occupied by the binder to the available pore volume, was calculated using Eq. (2):

$$S = \frac{V_{\text{binder}}}{V_{\text{pores}}} = \frac{w_0 m_{0,\text{sample}} - m_{\text{sample}}}{\rho_s E_1 \pi L R^2} \quad (2)$$

where S is the degree of saturation, V_{binder} [m^3] is the volume of the binder in the sample, V_{pores} [m^3] is the volume of all pores (space between particles) in the sample, w_0 is the weight part of the binder in the sample before debinding, $m_{0,\text{sample}}$ [kg] is the mass of the sample before debinding, m_{sample} [kg] is the mass of the sample after debinding, ρ_s [kg/m^3] is the density of the binder in the solid state, E_1 is the porosity of the sample, L[m] is length of the sample and R[m] is the radius of the sample.

The degree of saturation was in the range of 92–95% inside the binder-rich region and 60% in the binder-lean core. The porosity was calculated from the mass and the volume of the samples with completely removed binder by burnout at 650 °C in air:

$$E_1 = 1 - \frac{m'}{\pi L R^2 \rho_{\text{powder}}} \quad (3)$$

where m'[kg] is the mass of the moulded piece with completely removed binder and ρ_{powder}[kg/m^3] is the density of the ceramic powder.

The pore structure in both regions is thus in a funicular state, which is typical for a degree of saturation above 24% for polydisperse powders.[12] The amount of binder in each region was found to be constant throughout the progress of the debinding – thus the samples were losing weight due to a decrease in the thickness of the binder-rich region.

The quenching test revealed that at temperatures above the melting point of the binder there exists a film of molten binder on the surface of the moulded pieces. Flakes of mostly pure wax are visible on the surface of the piece that was quenched from a temperature above the melting point of the binder (Fig. 2). This indicates that the molten binder is exuded from the sample, while

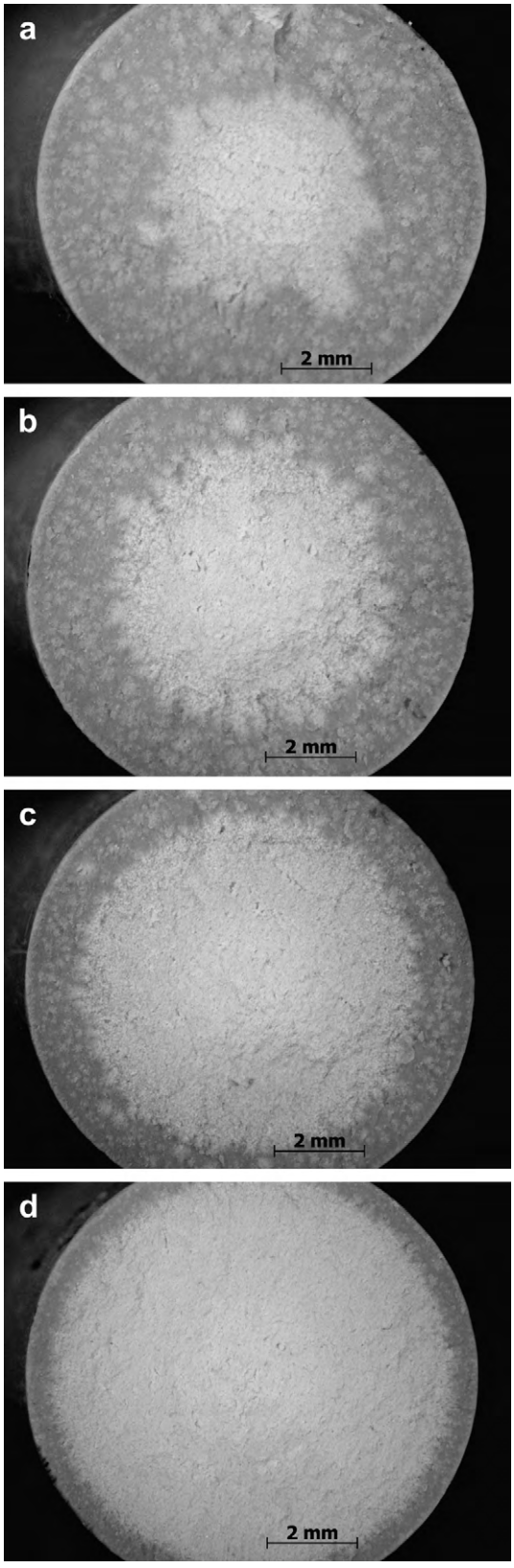

Fig. 1. Photographs of the fracture surfaces of moulded pieces at different debinding times, (a) 85 min, (b) 150 min, (c) 250 min and (d) 540 min. A linear temperature regime with a ramp = 0.7 K/min and a dwell temperature = 130 °C were used. There is a clearly seen binder-lean core in the center (light grey), surrounded by a binder-rich region (darker grey).

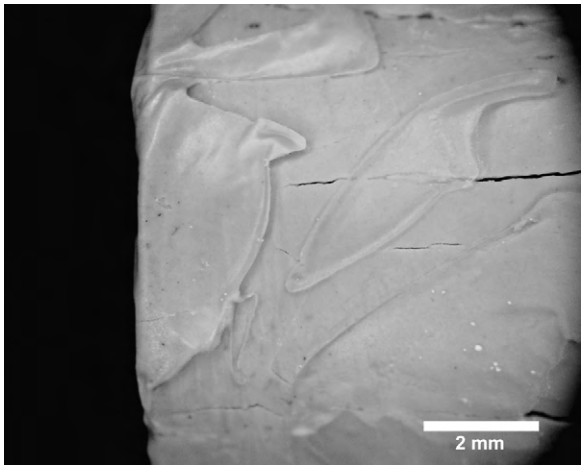

Fig. 2. Picture of the sample that was quenched in liquid nitrogen from a temperature above the melting point of the binder.

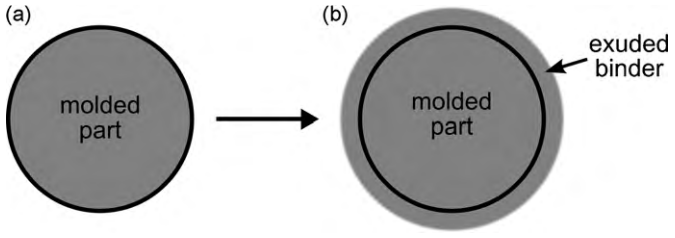

Fig. 3. A sketch describing the exudation effect. When a body saturated with the binder (a) is heated above the melting point, the binder melts and is exuded into the surroundings (b).

the sample itself remains undeformed. The sample cracked due to the thermal shock during quenching.

4. Theoretical considerations

Comparing our observations with the predictions of existing models shows that none of these models can satisfactorily describe the particular process. We clearly observed a front-like movement of the binder, which is not consistent with the majority of models. In this respect, German's model[2] seems to be correct; however, our experiments show that only a minor part of the binder moves in a front-like movement – a fact that is not described by German's model. Furthermore, an additional mechanism contributes to the debinding process, i.e., the exudation of the binder due to thermal expansion. We used German's model as a basis, but we took into account additional assumptions. The following assumptions reflect mechanisms that are important during the process of wick-debinding:

(i) The powder skeleton of the moulded piece is rigid and does not deform throughout the process. Also, the piece does not change in size.
(ii) The binder expands with increasing temperature. A large, and relatively sudden, expansion occurs when the binder melts. However, because the powder skeleton does not deform, this causes the binder to be exuded from the body, as sketched in Fig. 3. The binder "exudation effect" was already observed[7,13] and considered[7] for the wax-zirconia system.
(iii) A pressure gradient arises due to the wetting of the highly porous powder embedment. Darcy's law describes the flow of a molten binder through the sample and the wick embedment.
(iv) The binder inside the piece is located in two different states: as a mobile binder in the larger voids between powder particles, which can flow due to the pressure gradient; and as an immobile binder located on the surfaces of the particles and inside the smaller voids, which cannot be moved due to the capillary suction – it is too strongly bonded to the powder (see Fig. 4). This differentiation is based only on position, not on the chemical nature of the binder.
(v) The binder inside the wick embedment is moving as a column with a sharp leading front. This kind of movement has been already described by some authors who studied the movement in wicking embedment in more detail.[6,7]
(vi) When the binder cools and solidifies it contracts. This causes a significant rearrangement of the binder distribution, because the mobile part can still move before it completely solidifies.

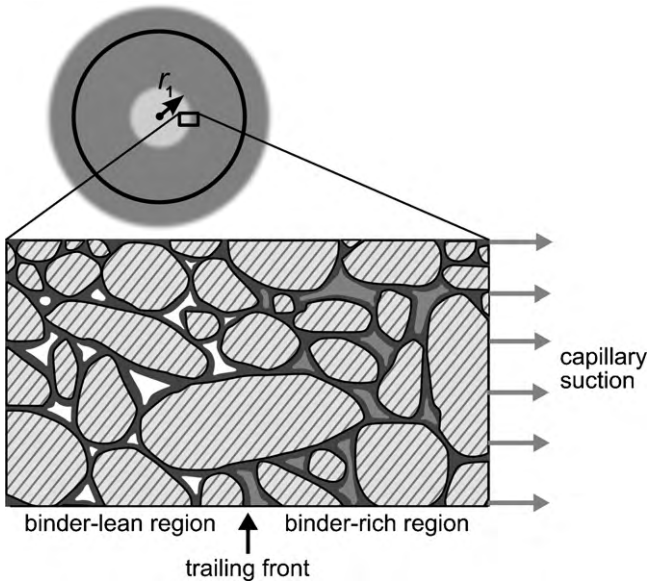

Fig. 4. A sketch of the binder distribution during debinding. When a body with molten binder is in contact with the wicking powder, capillary suction causes the mobile part of the binder to move toward the wicking agent. Some of the binder (the immobile part, marked as dark-gray around the particles) stays behind, trapped inside the fine pores and the particle surfaces. A trailing front, located at a distance r_1 from the center, is gradualy moving toward the edge of the moulded piece.

5. Theoretical model

The described assumptions must be explicitly formulated in order to construct a mathematical model used to quantitatively compare the theory with experiments. The discussion of the model is divided into four parts. Two mechanisms of binder removal are discussed first, i.e., the capillary extraction and the exudation effect, which are then combined to obtain a complete

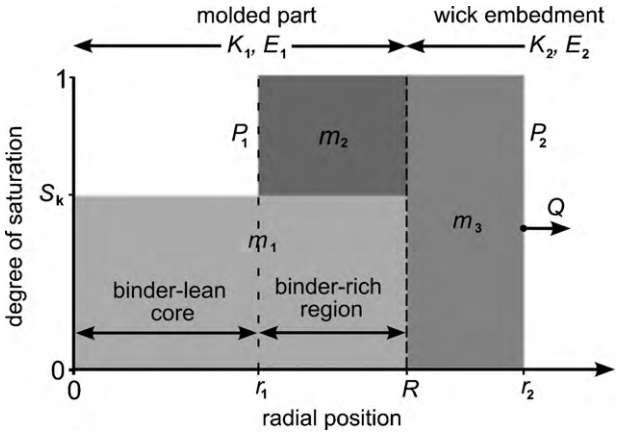

Fig. 5. A sketch of the binder distribution during thermal debinding as a function of radial position. Up to the critical degree of saturation (S_k), the binder is immobile (m_1). The mobile part of the binder (m_2) is moving from the moulded piece into the surrounding wick embedment. The binder that has already penetrated into the wicking embedment is marked as m_3.

description of the binder's removal. Finally, a mechanism of binder redistribution during cooling is discussed.

5.1. The capillary extraction

Capillary extraction can be described using Darcy's law. The equation for the cylindrical shape is:

$$Q = -2\pi r L \frac{K}{\eta}\frac{dP}{dr} \tag{4}$$

where Q[m^3/s] is the volumetric flow, r[m] is the radial distance from the center of the moulded piece, L[m] is the length of the body, K[m^2] is the permeability, η[Pa s] is the viscosity and dP/dr[Pa/m] is the pressure gradient.

In our case the binder is moving through two different domains – the moulded piece and the surrounding wick embedment – which have different permeabilities (see the sketch in Fig. 5). The movement of the mobile part (m_2) of the binder can be written as:

$$\int_{r_1}^{R} Q\frac{\eta dr}{K_1 r} + \int_{R}^{r_2} Q\frac{\eta dr}{K_2 r} = -2\pi \int_{P_1}^{P_2} L dP \tag{5}$$

where K_1[m^2] is the permeability inside the moulded piece, K_2[m^2] is the permeability in the wicking embedment, r_1[m] is the distance of the trailing front from the center, r_2[m] is the distance of the leading front from the center and R[m] is the radius of the piece.

As a result of integrating Eq. (5) we obtain:

$$Q\left[\frac{\eta}{K_1}\ln\left(\frac{R}{r_1}\right) + \frac{\eta}{K_2}\ln\left(\frac{r_2}{R}\right)\right] = -2\pi L\Delta P \tag{6}$$

The mass flow can be written in the form of a difference equation in order to solve it numerically:

$$Q = \frac{dm_3}{\rho dt} \approx \frac{\Delta m_3}{\rho \Delta t} \tag{7}$$

where m_3[kg] is the mass of the binder that has penetrated into the wicking embedment in the small time increment Δt[s] and ρ[kg/m^3] is the density of the binder.

From Eqs. (6) and (7) a difference equation for the mass change due to capillary pressure is obtained:

$$\Delta m_{\text{capillar}} = -\frac{2\pi\rho L K_2 \Delta P}{\eta[K_2/K_1\ \ln(R/r_1) + \ln(r_2/R)]}\Delta t \tag{8}$$

5.2. Exudation of the binder due to thermal expansion

In the beginning of the process the binder occupies all the available space between the particles ($S = 1$). The mass of the binder at the beginning of the process is:

$$m_0 = \rho_s E_1 \pi L R^2 \tag{9}$$

where ρ_s[kg/m^3] is the density of the solidified binder.

When the binder is in the molten state, two forms of the binder can be distinguished inside the moulded piece – the mobile and the immobile part. The immobile part of the binder in the piece is located around the particles and inside the finer pores throughout the piece. The binder preferentially occupies the smaller pores, but if the degree of saturation is above a certain critical level (S_k), then all the positions of the immobile binder are filled and some binder is located in larger pores, where it can easily move – this binder is called the mobile binder. The amount of immobile binder can be calculated, according to the schematic drawing in Fig. 5:

$$m_1 = \rho S_k E_1 \pi L R^2 \tag{10}$$

where m_1[kg] is the total mass of the immobile part of the binder, S_k[/] is the critical degree of saturation level (the binder above S_k is mobile and below S_k is immobile).

Because the total mass of the binder in the system is constant, the mobile part of the binder can be calculated from the total mass of the binder (m_0) and the masses of the binder located in other places, i.e., m_1 and m_3, as is written in Eq. (11) (see sketch in Fig. 5). Eqs. (9) and (10) are used to further develop Eq. (11):

$$m_2 = m_0 - m_1 - m_3 = E_1 \pi L R^2(\rho_s - \rho S_k) - m_3 \tag{11}$$

where m_2[kg] is the mass of the mobile part of the binder inside the piece, m_0[kg] is the total mass of the binder and m_3[kg] is the mass of the binder inside the wick embedment (one that has already left the piece).

The moulded piece does not change its dimensions during debinding, so the volume of the space between the particles is constant. There exists a maximum amount of binder that can be located inside this space – when the binder occupies all of the voids between particles ($S = 1$). The moulded piece is then fully saturated with the binder (this is the state at the beginning of the process):

$$m_{\max} = \rho E_1 \pi L R^2 \tag{12}$$

where $m_{\max}$[kg] is the maximum amount of binder that can be located inside the moulded piece, when the binder is in the molten state.

If the moulded piece is saturated with the binder ($S=1$), the thermal expansion would build up an excess amount of binder inside the piece. Because of the incompressibility of the molten binder the excess of the binder is exuded from the piece:

$$\Delta m_{\text{excess}} = (m_1 + m_2) - m_{\max} \tag{13}$$

where Δm_{excess}[kg] is the excess amount of binder inside the moulded piece that has built up in the time increment of Δt[s].

Combining Eq. (13) with Eqs. (10)–(12) we obtain:

$$\Delta m_{\text{excess}} = E_1 \pi L R^2 (\rho_s - \rho) - m_3 \tag{14}$$

5.3. Combining the debinding mechanisms

Both mechanisms, the capillary extraction and the exudation, contribute to the binder loss. Putting it another way, both mechanisms cause an increase in the amount of binder that has escaped into the wicking embedment (m_3):

$$m_3(t + \Delta t) = m_3(t) + \Delta m_{\text{capillar}} + \Delta m_{\text{excess}} \tag{15}$$

where $m_3(t+\Delta t)$[kg] is the mass of the binder in the wick after a small time increment Δt[s] and $m_3(t)$ is the mass of the binder in the wick before the small time increment Δt. When we combine Eq. (15) with Eqs. (8) and (14) we obtain the central equation of the model, which describes the kinetics of the mass transport, considering both mechanisms:

$$m_3(t + \Delta t) = m_3(t) + \frac{2\pi\rho L K_2 \Delta P}{\eta[K_2/K_1 \ \ln(R/r_1) + \ln(r_2/R)]}\Delta t + [E_1 \pi L R^2 (\rho_s - \rho) - m_3(t)] \tag{16}$$

However, the equation has some conditions that we must consider in the calculation. The second part on the right-hand side of the equation, describing capillary extraction, is only valid when there is some amount of mobile part present inside the piece (if $m_2 > 0$), otherwise it is zero. The last part on the right-hand side of the equation, describing the removing of the binder due to exudation, is considered only if it has a positive value, otherwise it is zero; because the last condition, the first part on the left-hand side of the equation, cannot cancel out with $m_3(t)$ inside the third part.

The trailing front r_1, used in Eq. (16), is calculated according to the sketch in Fig. 5. It is derived from the statement that the mass of the mobile part (m_2) is located between the trailing front (r_1) and the edge of the sample (R), inside the space between the particles that are not already occupied by the immobile binder (m_1). Eq. (11) is used to replace m_2:

$$r_1 = \sqrt{R^2 - \frac{m_2}{\rho E_1 (1 - S_k)\pi L}} = \sqrt{R^2 - \frac{E_1 \pi L R^2 (\rho_s - \rho S_k) - m_3(t)}{\rho E_1 (1 - S_k)\pi L}} \tag{17}$$

The leading front r_2, used in Eq. (16), is also calculated according to the sketch in Fig. 5:

$$r_2 = \sqrt{R^2 + \frac{m_3(t)}{\rho E_2 \pi L}} \tag{18}$$

The density and the viscosity in Eq. (16) are temperature dependent. For the viscosity we used the exponent dependency:

$$\eta = A \ \exp\left(\frac{b}{T} - c\right) \tag{19}$$

where A[Pa s], b[°C] and c are experimentally obtained constants.

A linear regression was used to describe the temperature dependency of the density of the binder in the molten state:

$$\rho = \rho_s; \text{ if } T < \text{melting point} \tag{20a}$$

$$\rho = \rho(60\ ^\circ\text{C}) + a\,T; \text{ if } T > \text{melting point} \tag{20b}$$

where $\rho(60\,^\circ\text{C})$ and a [kg/°C m^3] are experimentally obtained constants. The temperature (T) is time dependant and is calculated from Eqs. (1a) and (1b).

The set of Eqs. (16)–(18), together with Eqs. (19), (20a) and (20b), constitute the model describing the mass transport of the binder during thermal wick-debinding. These equations are solved numerically, calculating Eqs. (16)–(20b) step by step, discretely increasing the time for Δt in each step, as is evident from Eq. (16). The initial conditions, such as $m_3(0)$, $r_1(0)$, $r_1(0)$ at time $t=0$, are known and are obtained experimentally. An accurate numerical solution of m_3 as a function of time can be calculated if a small enough Δt is used. In our calculations we used $\Delta t = 5$ s. The code was written and executed in Scilab software.

For each time a binder content inside the moulded piece can be calculated:

$$w = \frac{m_1 + m_2}{m_1 + m_2 + m_{\text{powder}}} = \frac{m_1 + m_2}{m_1 + m_2 + \rho_{\text{powder}} E_1 \pi L R^2} \tag{21}$$

where m_{powder}[kg] is the mass of ceramic powder inside the sample and ρ_{powder} is the density of the powder.

5.4. Redistribution of the binder during cooling

When the process of thermal debinding is stopped, the remaining binder cools and then finally solidifies or freezes. However, this has no effect on the binder content, but it does have a significant effect on the binder distribution inside the piece.

When the binder freezes it contracts, and since the mobile binder can move, the whole continuous body of the mobile binder contracts. It contracts towards the edge of the moulded piece, because the solidification is happening from the outside towards the inside. The immobile part of the binder freezes in its location and does not shift position. The trailing front after the solidification ($r_{1,s}$) is calculated using Eq. (22), which is similar

to Eq. (17), except that the density of the binder (ρ) is changed to the density in the solid state (ρ_s). Because ρ_s is larger than ρ, it follows that $r_{1,s}$ is larger than r_1; the frozen trailing front is located closer to the edge of the sample than was the trailing front in the molten state:

$$r_{1,s} = \sqrt{R^2 - \frac{m_2}{\rho_s E_1 (1 - S_k)\pi L}} \quad (22)$$

where $r_{1,s}$[m] is the distance of the frozen trailing front from the centre of the sample. The thickness of the binder-rich region after the solidification (d[m]) is:

$$d = R - r_{1,s} \quad (23)$$

6. Discussion

In order to verify our model, we quantitatively compared the experimental data and the model. The binder content and the thickness of the binder-rich region vs. time were compared with the model's prediction. The input parameters used in the model were: $E_1 = 0.372$ or 0.368 (for the suspension A with 87.8% and suspension B with 88.0% suspensions, respectively), $E_2 = 0.70$ and the binder melting point = 60 °C. The density of the ceramic powder was 3900 kg/m^3. The density of the binder below the melting point (ρ_s) is 920 kg/m^3, while the density above the melting point was interpolated with Eq. (20b), based on the graduated cylinder measurements. The parameters used to best fit the data were $\rho(60\,^\circ\text{C}) = 815$ kg/m^3 and $a = 0.58$ kg/(°C m^3). The viscosity of the binder above the melting point was interpolated with Eq. (19), based on the rheometer measurements. The parameters used to best fit the experimental data were $A = 0.0095$ Pa s, $b = 195\,^\circ$C and $c = 3$. Two of the parameters, $\Delta P \times K_2 = 7 \times 10^{-15}$ Pa m^2 and $S_k = 0.75$, were chosen to best fit the experimental data of the binder content obtained from debinding tests with suspension A (87.8% powder). The best fitting occurred when the permeability of sample was much larger than the permeability of the embedment (ratio $K_2/K_1 \to 0$). The same values were then used to simulate the debinding of suspension B (88.0% powder), for all the temperature regimes. Both of these parameters are difficult to determine experimentally with sufficient accuracy. Those parameters actually present the result of the theoretical analysis and, taking into account the model, gives us information about the conditions inside the sample during the process, which is very difficult to observe experimentally.

The moulded pieces retained their size and shape after the debinding cycle. The technical linear shrinkage was below 0.1%. This is consistent with the work of Wright et al.[14] who observed that the shrinkage is inversely related to the ceramic volume fraction and that very little shrinkage occurs at a volume fraction of around 64%.

The model predictions are presented on graphs as lines, together with the experimentally obtained values, marked as diamond-shaped points (each point represents one sample). We found that, according to the model, the permeability is far greater in the ceramic body than in the wicking embedment. Therefore, all the resistance to flow is in the wick embedment, and the resistance inside the moulded pieces can be neglected.

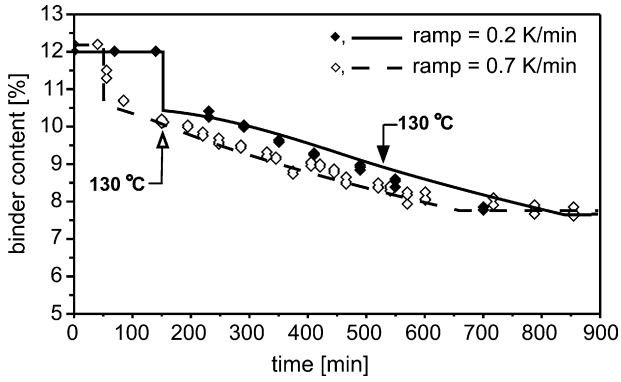

Fig. 6. Binder content as a function of the time of debinding. The time when the temperature reached the dwell temperature of 130 °C is marked for both temperature regimes.

The model confirms that the discrete loss of binder at the beginning is caused by the exudation of the binder during melting. The density of the binder decreases from 0.92 g/cm^3 in the solid state to 0.783 g/cm^3 just above the melting point, which causes the binder to exude out of the sample. The amount of binder loss due to this effect agrees well with the experiments. The effect is seen in a discrete, sudden drop in the amount of binder content at the beginning (Figs. 6 and 8). This effect also has consequences for the binder distribution – a binder-depleted core forms as the binder solidifies. This is seen as a drop in the thickness of the binder-rich region at the beginning (in the beginning the thickness of the binder-rich region is equal to the sample radius) (Figs. 7 and 9). Again, the model calculations match well with the experimental data. Our observations, that only a relatively small part of the binder moves due to the capillary suctions, is quantitatively determined using the model – only 25% of the molten binder moves and 75% ($S_k = 0.75$) of the binder is immobile. S_k depends on the pore size distribution in moulded parts and in the wicking embedment. In our particular case, a high solids loading of micron sized particles in the moulded part and a wicking embedment with high specific surface was used, resulting in very strong capillary suction.

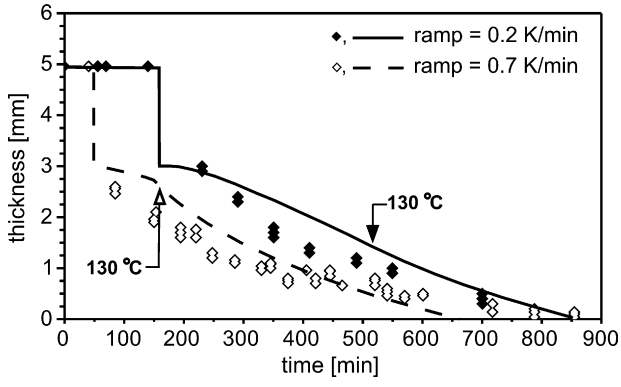

Fig. 7. The thickness of the binder-rich region (d) as a function of the time of debinding. The time when the temperature reached the dwell temperature of 130 °C is marked for both temperature regimes.

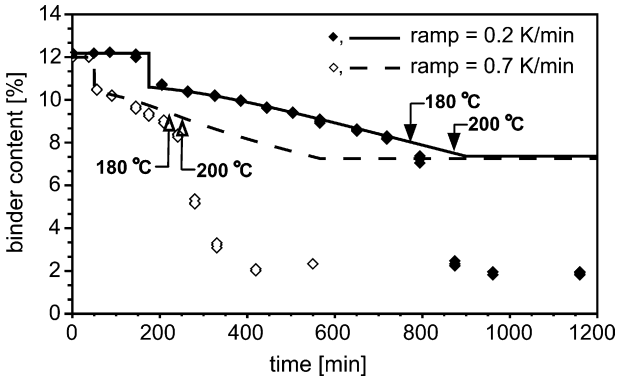

Fig. 8. Binder content as a function of the time of debinding. The time when the temperature reached the dwell temperature of 200 °C is marked for both temperature regimes. The time when temperature 180 °C was reached is also marked; above this temperature the oxidation process prevails as a debinding mechanism.

Such a combination was not used by some researchers and this is presumably the reason why they[7] did not observe front-like extraction. After the initial phenomena, connected with the melting of the binder, a gradual decrease in the binder content and the thickness of the binder-rich region takes place, which is consistent with capillary extraction, described by Darcy's law. This holds for all kinds of temperature regimes until the temperature is below 180 °C. We found that if the temperature during debinding exceeds 180 °C an exothermic reaction takes place, which significantly accelerates the binder removal rate. At higher temperatures the binder oxidizes in a complex chemical reaction; it is partially transformed into a volatile product and partially into a non-volatile, brown-colored, solid substance.[15] Since the model does not describe such a phenomenon, the calculated lines deviate from the experimental data when the temperature exceeds 180 °C. This can be seen in Figs. 8 and 9 where the dwell temperature was 200 °C.

The chemical reaction has an important role in the debinding process, especially in the final stage of debinding, in which a complete removal of the binder must occur before the sintering takes place. But partial capillary extraction must first be completed, so that open porosity is introduced into the moulded piece. Without that porosity, the volatile products of oxidation would not be able to escape quickly enough and the pieces would be damaged. However, the details of this are beyond the scope of this paper.

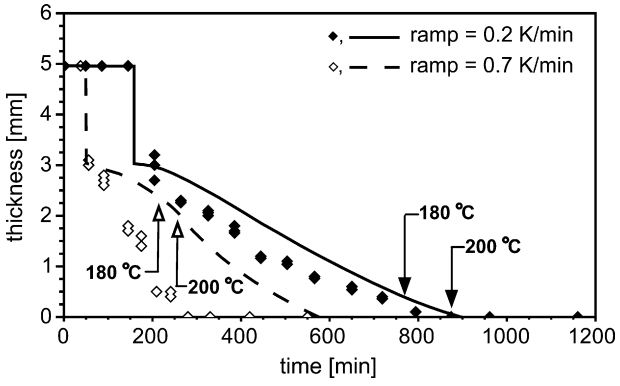

Fig. 9. The thickness of the binder-rich region (d) as a function of the time of debinding. The time when the temperature reached the dwell temperature of 200 °C is marked for both temperature regimes. The time when the temperature of 180 °C was reached is also marked; above this temperature the oxidation process prevails as a debinding mechanism.

7. Conclusions

Our experimental work confirms that in a system of fine Al_2O_3 ceramic powder and a paraffin-based binder a characteristic binder distribution with a binder-rich region below the surface, surrounding an inner, binder-depleted region, does actually form during the thermal wick-debinding. The border between the regions is sharp. We also observed a large decrease in the binder content at the beginning of the process, where the temperature just exceeds the melting point of the binder. Based on the observed data, mechanisms of thermal wick-debinding were proposed and a model was constructed to test the mechanisms. Because the model predictions are consistent with the experimental data, this argues in favor of the correctness of the proposed mechanisms.

This means that the single-component binder inside the moulded pieces exists in two different forms – as an immobile binder, strongly bonded by the powder inside the finer pores, and as a relatively mobile binder, located in the larger pores. Only the mobile part of the binder can move due to capillary suction; according to our model this amount is 25%. The model also indicates that the resistance to flow of the molten binder is far greater in the wick embedment than inside the moulded piece. The large drop in the binder content at the beginning of the process is explained by a change in the density of the binder when it melts. Because the powder skeleton is rigid and does not deform, the expanding binder is exuded from the moulded piece. Furthermore, if the temperature during the debinding exceeds 180 °C, an oxidation reaction prevails as a mechanism of the binder removal.

References

1. German RM. *Powder injection molding – design and applications*. State College, Pennsylvania: Innovative Material Solutions, Inc.; 2003.
2. German RM. Theory of thermal debinding. *Int J Powder Met* 1987;**23**:237–45.
3. Vetter R, Horninge WRB, Vervoort PJ, Glabus IM, Zhuang LZ, Duszczyk J. Square foot debinding model for powder injection moulding. *Powder Metall* 1994;**37**:265–71.
4. Vetter R, Sanders MJ, Glabus IM, Zhung LZ, Duszczyk J. Wick–Debinding in powder injection molding. *Int J Powder Metall* 1994;**30**(1):115–24.
5. Bao Y, Evans JRG. Kinetics of capillary extraction of organic vehicle from ceramic bodies. Part I: flow in porous media. *J Eur Ceram Soc* 1991;**8**:81–93.
6. Bao Y, Evans JRG. Kinetics of capillary extraction of organic vehicle from ceramic bodies. Part II: partitioning between porous media. *J Eur Ceram Soc* 1991;**8**:95–105.
7. Somasundram IM, Cendrowitz A, Wilson DI, Johns ML. Phenomenological study and modelling of wick debinding. *Chem Eng Sci* 2008;**63**:3802–9.
8. Shih MS, Houring LW. Numerical simulation of capillary-induced flow in a powder-embedded porous matrix. *Adv Powder Technol* 2001;**12**(4):457–80.

9. Lin TL, Houring LW. Investigation of wick debinding in metal injection molding: numerical simulations by the random walk approach and experiments. *Adv Powder Technol* 2005;**16**(5):495–515.
10. Kim SW, Lee HW, Song H, Kim BH. Pore structure evolution during solvent extraction and wicking. *Ceram Int* 1996;**22**:7–14.
11. Kim SW, Lee HW, Song H. Effect of minor binder on capillary structure evolution during wicking. *Ceram Int* 1999;**25**:671–6.
12. German RM. *Powder injection molding*. New Jersey: Metal Powder Industries Federation; 1990.
13. Song JH, Evans JRG. Flocculation after injection molding in ceramic suspensions. *J Mater Res* 1994;**9**:2386–97.
14. Wright JK, Edirisinghe MJ, Zhang JG, Evans JRG. Particle packing in ceramic injection molding. *J Am Ceram Soc* 1990;**73**:2653–8.
15. Zorzi JE, Perottoni CA, Da Jornada AH. Hard-skin development during binder removal from Al_2O_3-based green ceramic bodies. *J Mater Sci* 2002;**37**:1801–7.